WHOI-89-11

(2)

Woods Hole Oceanographic Institution

The 17-Meter Flume at the Coastal Research Laboratory. Part II: Flow Characteristics

by

John H. Trowbridge, W. Rockwell Geyer,
Cheryl Ann Butman, and Robert J. Chapman

May 1989

Technical Report

Funding was provided by the Minerals Management Service under contract Number 14-12-0001-30262; Sea Grant under contract Number NA86-AA-D-FG090; the Office of Naval Research Young Investigator Program under contract Number N00014-86-K-0579.

CRC-89-3
Coastal Research Center

WHOI-89-11

The 17-Meter Flume at the Coastal Research Laboratory. Part II: Flow Characteristics

by

John H. Trowbridge, W. Rockwell Geyer,
Cheryl Ann Butman, and Robert J. Chapman

Woods Hole Oceanographic Institution
Woods Hole, Massachusetts 02543

May 1989

Technical Report

Funding was provided by the Minerals Management Service under contract Number 14-12-0001-30262; Sea Grant under contract Number NA86AA-D-FG090; and the Office of Naval Research Young Investigator Program under contract Number N00014-86-K-0579.

 This report should be cited as: Woods Hole Oceanog. Inst. Tech. Rept., WHOI-89-11. CRC-89-3.

Approved for publication; distribution unlimited.

Approved for Distribution:

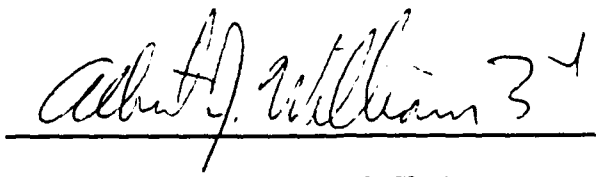

Albert J. Williams 3rd, Chairman
Department of Applied Ocean Physics and Engineering

THE 17-METER FLUME AT THE COASTAL RESEARCH LABORATORY. PART II: FLOW CHARACTERISTICS

John H. Trowbridge,
W. Rockwell Geyer,
Cheryl Ann Butman and
Robert J. Chapman

Ocean Engineering Department
Woods Hole Oceanographic Institution
Woods Hole, Massachusetts 02543

ABSTRACT

This report summarizes the characteristics of the idealized one-dimensional turbulent channel flow for which the 17-Meter Flume was designed, and describes a measurement program designed to determine whether the flume can in fact produce such a flow. The measured quantities include mean velocities, Reynolds stresses, turbulence intensities and velocity spectra. Measured profiles of mean velocity, Reynolds stress and turbulence intensity are consistent with previous theoretical and empirical results. Measured spectra, although consistent with expectations over a wide range of frequencies, indicate a few unexpected features, including a constant spectral density at high frequencies (possibly due to aliasing or high-frequency noise), motion at a few well-defined high frequencies of order 10 hz (possibly due to structual vibrations), oscillations with time scales of order 30 s (possibly due to low-mode standing surface waves) and irregular motions with time scales of several minutes (possibly due to fluctuations in pump performance). The unexpected features indicated by the spectra at high and low frequencies do not have a significant effect on mean velocities and low-order statistics, but they may be important in some applications.

Contents

List of Figures

List of Tables

List of Symbols

Symbol	Definition
A	Empirical constant in equation (7)
b	Width of channel
B	Empirical function of $k_s u_*/\nu$ in equation (12)
B'	Empirical constant in equation (18)
D_u	Empirical constant in equation (15)
D_w	Empirical constant in equation (16)
f	Empirical function of zu_*/ν in equations (6), (7) and (8)
f'	Empirical function of z/k_s and $k_s u_*/\nu$ in equation (12)
F_g	Gravitational force in Figure 2
F_v	Force due to viscous stress in Figure 2
g	Gravitational acceleration
h	Depth of channel flow
k_s	Equivalent Nikuradse sand roughness of channel bottom
ℓ	Scale of turbulent eddy
L	Spatial separation in spatial correlation function
M	Momentum flux in Figure 2
N	Number of data points in a sample
r^2	Normalized correlation coefficient
R_{11}	Temporal correlation function defined by equation (23)

Symbol	Definition
R_{33}	Temporal correlation function defined by equation (24)
S_{11}	Frequency spectrum defined by equation (25)
S_{33}	Frequency spectrum defined by equation (26)
t	Time
t_*	Averaging time defined in equation (31)
T	Temporal lag in temporal correlation function
u	x-component of velocity
$\overline{u}$	Mean value of u
u'	Fluctuating component of u
u_*	Shear velocity
$\hat{u}$	Average velocity defined in equation (31)
U	Depth-averaged mean velocity
w'	Fluctuating part of the z-component of velocity
W	Wake function in equations (6) and (9)
x	Along-channel coordinate
y	Cross-channel coordinate
z	Coordinate normal to channel bottom
z_+	zu_*/ν
z_o	Wall roughness length defined in equations (13) and (14)
z'	Displaced vertical coordinate defined in equation (32)
α_1	Empirical constant in equation (29)

Symbol	Definition
α_3	Empirical constant in equation (30)
γ	Empirical constant in equation (8)
Γ	Empirical function of zu_*/ν in equation (18)
δ_v	Empirical constant in equation (8)
Δ	Displacement of vertical coordinate in equation (32)
ε	Dissipation of turbulent kinetic energy per unit mass
θ	Slope of channel bottom with respect to horizontal
κ	Karman constant
λ_u	Empirical constant in equation (15)
λ_w	Empirical constant in equation (16)
ν	Kinematic viscosity
ξ	z/h
Π	Coles parameter
ρ	Density
τ	Shear stress (viscous stress plus Reynolds stress)
τ_b	Bottom shear stress
ϕ_{11}	Spatial correlation function defined in equation (19)
ϕ_{33}	Spatial correlation function defined in equation (20)
ψ_{11}	Wavenumber spectrum defined in equation (21)
ψ_{33}	Wavenumber spectrum defined in equation (22)
ω	Radian frequency

1 INTRODUCTION

This report presents results of a measurement program designed to evaluate the performance of the 17-Meter Flume, located in the Coastal Research Laboratory at the Woods Hole Oceanographic Institution. A companion report (Butman and Chapman, 1989) gives a comprehensive description of the geometry of the flume, the associated hardware and instrumentation, the data acquisition and preliminary processing systems, and procedures for operation.

The 17-Meter Flume is designed to have a long working section in which one can produce a turbulent flow with mean properties that are approximately independent of time, independent of along-channel position, and, at least near the channel centerline, independent of cross-channel position. This type of flow is one-dimensional in the sense that mean quantities depend on only one spatial coordinate (perpendicular distance away from the bottom). The measurement program described here was designed to determine whether the 17-Meter Flume can in fact produce an approximately one-dimensional channel flow with the expected properties.

A brief description of the 17-Meter Flume is necessary for the purposes of this report. Figure 1 is a diagram of the flume. The raceway has a length of 17 m, a width of 60 cm, and a depth of 30 cm. The flow in the raceway is driven by gravity, and the bottom slope is adjustable by means of hydraulic jacks. Flow straighteners eliminate secondary currents at the upstream end of the raceway, and an adjustable weir at the downstream end provides depth control. The flow from the raceway can be channeled either directly into a sump, or into a settling basin, which ultimately leads to the sump. A centrifugal pump drives the flow from the sump through a return pipe to the upstream end of the raceway. Windows in the walls of the raceway allow optical measurements. The raceway currently has a smooth PVC false bottom.

The measurements described in this report were obtained with a two-axis forward-scattering laser-Doppler velocimeter (LDV), described by Agrawal and Belting (1988). The LDV is mounted on an automated traversing system, and it is oriented to measure velocity components in the $x - z$ plane (x is the along-channel coordinate, and z is normal to the floor of the channel). The LDV is currently configured to sample at a rate of 32 hz. Data acquisition and preliminary processing are carried out by a personal computer (see Butman and Chapman, 1989, for more details).

This report is organized as follows. Section 2 is a description of the idealized one-dimensional flow for which the 17-Meter Flume was designed. Section 3 describes the measurements that we obtained in the 17-Meter Flume, including a comparison with the idealized characteristics described in Section 2. Section 4 presents a summary and conclusions.

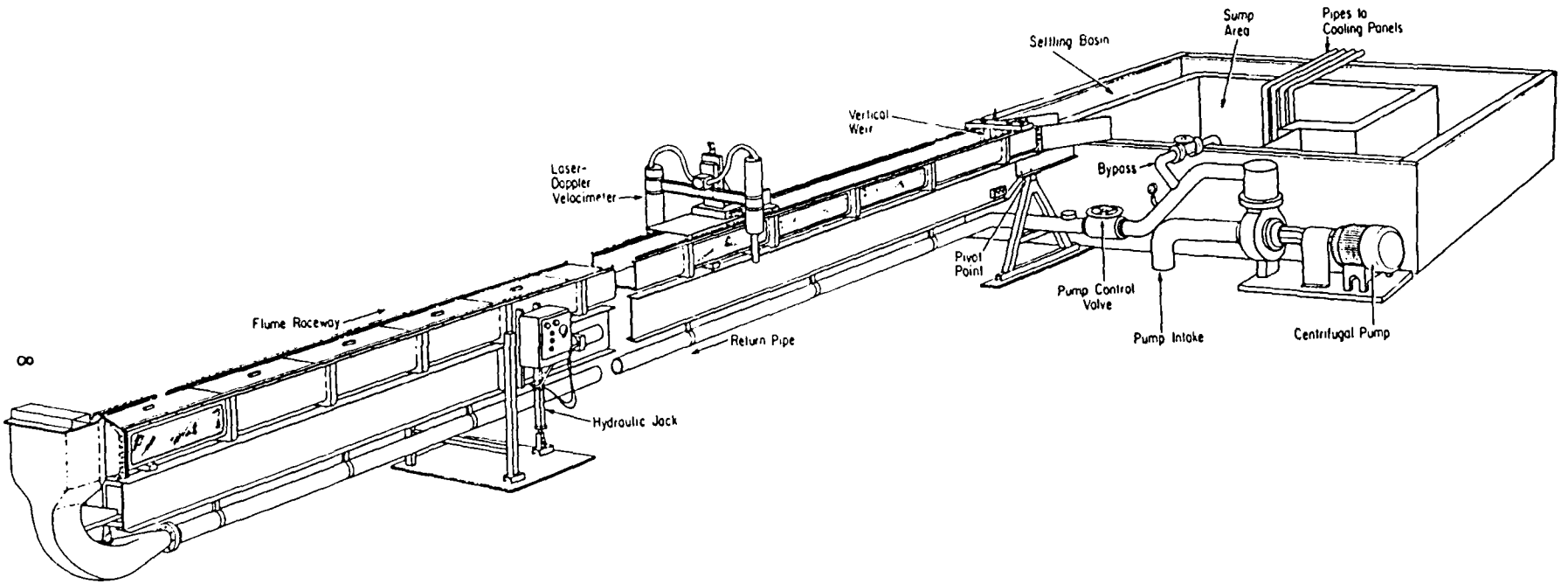

Figure 1: Diagram of the 17-Meter Flume.

2 BACKGROUND

In the case of clear water and a fixed smooth or rough bottom, the basic properties of one-dimensional turbulent flow in an open channel are well established by classical analyses (e.g. Millikan, 1939; Clauser, 1956; Coles, 1956) and experimental studies (e.g. Nezu and Rodi, 1986). A detailed description of the characteristics of one-dimensional channel flows can be obtained from several texts (e.g. Monin and Yaglom, 1971; Tennekes and Lumley, 1972; Hinze, 1975), and less rigorous accounts oriented toward biological and geological applications are also available (e.g. Komar, 1976; Nowell and Jumars, 1987). The present discussion is a brief summary of the basic results needed for the measurement program described in Section 3.

2.1 ESTABLISHMENT OF ONE-DIMENSIONAL FLOW

In order to produce a flow with mean properties that are approximately independent of along-channel position, one must set the discharge, bottom slope and downstream depth control properly (for a complete discussion of the hydraulic aspects of this problem, see for example Henderson, 1966). In most applications that are anticipated in the 17-Meter Flume, proper flume settings can be achieved by a fairly straightforward, although possibly time-consuming, iterative procedure (see Butman and Chapman, 1989).

In addition, in order to produce a flow that is approximately one-dimensional, an open channel must be sufficiently long (to allow the vertical structure to evolve from poorly constrained conditions at the channel entrance) and sufficiently wide (to eliminate the effects of the channel walls on the flow near the centerline). Simplified calculations based on the characteristics of turbulent boundary layers near flat plates (e.g. Schlichting, 1979), as well as conventional wisdom, suggest that the vertical structure of a turbulent open-channel flow is fully developed at distances greater than roughly 50 to 100 water depths downstream of the channel entrance. Based on laboratory measurements, Nakagawa et al. (1983) suggested that a turbulent open-channel flow is independent of cross-channel position at distances from the channel centerline less than about $(1/2)h[(b/h) - 4]$, where b is the channel width and h is the water depth. This information indicates that the 17-Meter Flume can in fact produce a long section in which the flow is approximately one-dimensional near the channel centerline, if the depth is less than about 15 cm.

2.2 DIMENSIONLESS PARAMETERS AND SCALES

The statistical properties of steady one-dimensional turbulent flow in an open channel are in principle determined completely by the mean bottom shear stress τ_b, the depth h, the kinematic viscosity ν, the gravitational acceleration g, the density ρ and the characteristics of the bottom. For simplicity we assume that the bottom is fixed and characterized completely by a single representative length, the Nikuradse equivalent sand roughness k_s (Schlichting, 1979).

According to the principles of dimensional analysis and dynamic similarity (e.g. Schlichting, 1979), the flow may alternatively be characterized by three dimensionless parameters, which may be chosen in several ways. Here we use the Froude number $U/(gh)^{1/2}$, the Reynolds number u_*h/ν, and the roughness Reynolds number u_*k_s/ν. The quantity u_* is the shear velocity, equal to $(\tau_b/\rho)^{1/2}$, and U is the depth-averaged mean velocity, which is in principle a unique function of τ_b, h, ν, ρ, g and k_s. We have chosen these particular dimensionless parameters because of their physical significance, discussed below.

The Froude number is the ratio of the depth-averaged flow speed to the propagation speed of long, small-amplitude surface waves. Although the Froude number is in general an important parameter characterizing open-channel flows (e.g. Henderson, 1966), it does not have a significant effect on the vertical structure of the flow if the mean properties are truly steady and independent of streamwise position, as assumed in the present discussion. It is worth noting, however, that at Froude numbers very near unity the free surface may respond dramatically to small irregularities in the bottom slope. In addition, the flow may be unstable to transient surface waves if the Froude number is greater than roughly two. Therefore, steady, fully developed flows may be difficult to establish at some values of the Froude number.

The Reynolds number u_*h/ν is roughly proportional to the ratio of inertial to viscous effects in the large-scale energy-containing turbulent eddies. If u_*h/ν is sufficiently large (greater than roughly one thousand), viscosity has a direct effect on the mean motion and the large-scale eddies only in a thin viscous sublayer near the bottom, which has a thickness of order $10\nu/u_*$. At large u_*h/ν, the mean motion and large-scale fluctuations outside of the viscous sublayer are essentially independent of u_*h/ν, so that the precise value of the Reynolds number may be unimportant for many purposes.

The roughness Reynolds number is proportional to the ratio of the roughness scale to the thickness of the viscous sublayer. If the roughness Reynolds number is less than about five, the roughness has no significant effect on the flow, so that the bottom is effectively smooth. If the roughness Reynolds number is greater than about seventy, the viscous sublayer is completely disrupted, and the viscosity has very little direct effect on the mean flow or the large-scale fluctuations.

Outside of the region very near the bottom that is directly affected by viscosity and the detailed geometry of the roughness elements, the turbulent motion spans a wide range of spatial scales. The energetic eddies responsible for most of the momentum transfer have an intensity of order u_*, and a length scale that is limited by the vertical extent of the flow, so that the length scale is roughly proportional to h. The much weaker velocity fluctuations responsible for viscous dissipation of energy have much smaller spatial scales, of order $h(u_*h/\nu)^{-3/4}$ (e.g. Tennekes and Lumley, 1972). The time required for an eddy with scale ℓ to be advected past a fixed point by the mean motion is of order ℓ/U. Therefore, a velocity record at a fixed measurement station obtained by an ideal sensor will have energetic fluctuations with a time scale of order h/U, and weaker fluctuations spanning a wide range of smaller time scales to a minimum of order $(h/U)(u_*h/\nu)^{-3/4}$. Fluctuations will also occur at time scales longer than h/U.

As an example typical of the 17-Meter Flume, we may consider flow of water at room temperature (20°C) over a smooth bottom, with a depth of 10 cm and a shear velocity of 2 cm/s. Under these conditions, the kinematic viscosity is 0.01 cm^2/s, the depth-averaged velocity is about 40 cm/s, the thickness of the viscous sublayer is about 0.05 cm, the scale of the energy-containing eddies is 10 cm, and the scale of the smallest eddies is about 0.03 cm. The time required for an energetic eddy to be advected past a fixed station is of order 0.25 s, and the time required for the smallest eddies to be advected past a fixed station is of order 0.001 s. Many instruments (e.g. the LDV in the 17-Meter Flume) have effective measurement volumes with dimensions larger than 0.03 cm. Therefore, these instruments cannot resolve the smallest scales in the flow considered here. The smallest time scales in records produced by these instruments are limited by the size of the measurement volume, rather than by the scale of the smallest eddies.

2.3 THE MEAN STRESS DISTRIBUTION

The distribution of the shear stress in a one-dimensional open-channel flow may be obtained by applying the momentum principle to the control volume shown in Figure 2. The control volume has unit length in the along-channel direction and unit width in the direction normal to the sketch. The bottom of the control volume is at a distance z away from the bottom, and the height of the control volume is $h - z$, where h is the water depth, as before. The along-channel coordinate is x, the bottom slope is θ, and gravitational acceleration is g, as before. Because of the assumption of one-dimensional flow, the water surface and the mean velocity are parallel to the bottom.

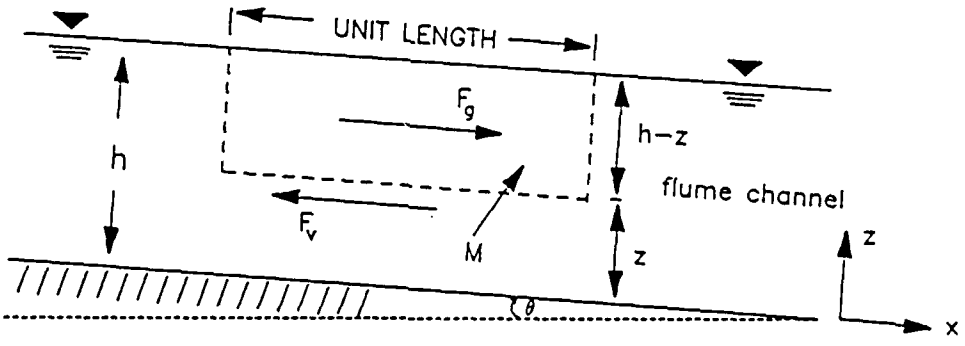

Figure 2: Control volume for analysis of the mean stress distribution in turbulent one-dimensional open-channel flow. The dashed lines indicate the control volume. F_g is the x-component of the gravitational force, F_v is the force due to the viscous shear stress, and M is the momentum flux across the bottom of the control volume.

According to the momentum principle, the mean force acting on the control volume and the mean momentum flux into the control volume must sum to zero. Because of the assumption of one-dimensional flow, the mean forces and momentum fluxes at the left and right ends of the control volume are identical, and therefore cancel and do not contribute to the mean momentum balance. The force due to the mean viscous stress acting on the bottom of the control volume is $\rho\nu(d\overline{u}/dz)$, where ρ and ν are the density and kinematic viscosity, as before, and $\overline{u}(z)$ is the mean along-channel velocity. The viscous stress acts in the negative x direction, so that it retards the fluid in the control volume. The x component of the gravitational force acting on the control volume is $\rho g \sin(\theta)(h - z)$. The gravitational force acts in the positive x direction, so that it would accelerate the fluid in the control volume in the absence of other effects. The mean momentum flux across the bottom of the control volume is $\rho\overline{u'w'}$. Here u' is the velocity fluctuation (instantaneous velocity minus mean velocity) in the x direction, w' is the velocity fluctuation in the z direction, and an overbar denotes a mean. Although there is no mean flow across the bottom of the control volume, there is a mean momentum flux, because u' and w' are correlated. If $\overline{u'w'}$ were positive, the mean momentum flux would add momentum to the fluid in the control volume. In reality, however, $\overline{u'w'}$ is negative, so that the mean momentum flux extracts momentum from the control volume.

By requiring the mean forces and momentum fluxes to sum to zero, we obtain

$$\rho\overline{u'w'} + \rho g \sin(\theta)(h - z) - \rho\nu\frac{d\overline{u}}{dz} = 0. \tag{1}$$

This expression can be rewritten:

$$\tau = \rho\nu\frac{d\overline{u}}{dz} - \rho\overline{u'w'} = \tau_b\left(1 - \frac{z}{h}\right). \tag{2}$$

Here τ is the total shear stress, equal to the sum of the viscous stress $\rho\nu d\overline{u}/dz$ and the Reynolds stress $-\rho\overline{u'w'}$ (actually a mean momentum flux due to turbulent velocity fluctuations, which acts like a stress). The quantity τ_b is the bottom shear stress, as before, given by

$$\tau_b = \rho g h \sin(\theta). \tag{3}$$

Equation (2) shows that the total shear stress varies linearly with distance above the bottom, and equation (3) shows that the bottom shear stress balances the down-slope component of the weight of the water column. Equation (2) may alternatively be written

$$-\rho\overline{u'w'} = \tau_b\left(1 - \frac{z}{h}\right) - \rho\nu\frac{d\overline{u}}{dz}. \tag{4}$$

By combining this expression with an equation for the mean velocity $\overline{u}(z)$ (see Section 2.4), one can obtain an expression for the Reynolds stress as a function of z. Well outside of the viscous sublayer (z greater than about $50\nu/u_*$), the second term on the right side of equation (4) is much smaller than the first, so that equation (4) approximates

$$-\rho\overline{u'w'} \simeq \tau_b\left(1 - \frac{z}{h}\right). \tag{5}$$

Equation (5) shows that the Reynolds stress varies approximately linearly with z well outside of the viscous sublayer.

The above analysis applies to steady, one-dimensional open-channel flows above both smooth and rough bottoms. If the bottom is smooth, $\overline{u'w'}$ must be zero at the bottom, so that the bottom stress is wholly a viscous shear stress. If the bottom is rough, the analysis breaks down within a few characteristic roughness lengths of the bottom, because of the assumption that the mean flow is parallel to the surface, which is not valid in the immediate vicinity of the roughness elements. The bottom stress on a rough bottom is transmitted in part by normal stresses acting on the sides of the roughness elements.

2.4 THE MEAN VELOCITY DISTRIBUTION

A general semi-empirical expression for the mean velocity in a steady, one-dimensional, open-channel flow above a smooth bottom is

$$\overline{u}(z) = u_* f(z_+) + u_* W(\xi) \tag{6}$$

(Nezu and Rodi, 1986). Here u_* is the shear velocity, as before, z_+ is zu_*/ν, ξ is z/h, and $f(z_+)$ and $W(\xi)$ are empirical functions.

In the inner part of the flow ($\xi = z/h$ less than about 0.2) the second term on the right side of equation (6) is much smaller than the first, and the velocity distribution is described by the wall function $f(z_+)$, which is the same in the wall region of any turbulent shear flow (e.g. channel flow, pipe flow, boundary layer flow) above a smooth surface (Clauser, 1956). Well inside of the viscous sublayer (z_+ less than about 5), $f(z_+)$ is approximately equal to z_+. Well outside of the viscous sublayer (z_+ greater than about 50), $f(z_+)$ is approximately logarithmic:

$$f(z_+) \simeq \frac{1}{\kappa} ln(z_+) + A \tag{7}$$

where κ is the empirical Karman constant and A is a second empirical constant. The commonly accepted values are $\kappa \simeq 0.40$ and $A \simeq 5.5$ (Nezu and Rodi, 1986). Reichardt (see Landahl, 1967) proposed the following empirical expression valid for all z_+:

$$f(z_+) = \frac{1}{\kappa} ln(1 + \kappa z_+) + \gamma[1 - exp\left(-\frac{z_+}{\delta_v}\right) - \left(\frac{z_+}{\delta_v}\right) exp(-0.33 z_+)] \tag{8}$$

where γ and δ_v are empirical constants. Landahl used $\delta_v = 11.0$ and $\gamma = 7.4$, which corresponds to $A = 5.1$ in equation (7). Here we use $\gamma = 7.8$ to correspond to the currently more commonly accepted value $A = 5.5$.

In the outer part of the flow ($\xi = z/h$ greater than about 0.2), the second term on the right side of equation (6), which is the wake correction introduced by Coles (1956), becomes significant. The shape of the wake correction is approximately the same for all wall-bounded turbulent shear flows, but its strength depends on the type of flow (e.g. the wake correction

is larger in a boundary layer with zero pressure gradient than it is in an open channel flow). An empirical expression for the wake correction $W(\xi)$ is

$$W(\xi) = \frac{2\Pi}{\kappa} \sin^2\left(\frac{\pi}{2}\xi\right) \tag{9}$$

(Coles, 1956) where Π is the empirical Coles parameter, which determines the strength of the wake correction. For steady, one-dimensional, open-channel flow Nezu and Rodi (1986) found that Π depends on the Reynolds number, increasing from a value of zero for hu_*/ν less than about 500 to a constant value of approximately 0.2 for hu_*/ν greater than about 2000.

The following commonly used logarithmic approximation to the mean velocity profile above a smooth wall may be obtained by neglecting the wake correction and using the approximation (7):

$$\overline{u}(z) \simeq \frac{u_*}{\kappa} ln\left(\frac{zu_*}{\nu}\right) + A. \tag{10}$$

Equation (10) is valid only in the relatively thin layer in which z is greater than about $50\nu/u_*$ but less than about $0.2h$.

Figure 3 shows a graph of the mean velocity profile in an open channel flow above a smooth bottom, based on equations (6), (8) and (9), for conditions typical of the 17-Meter Flume (a depth h of 10 cm, a shear velocity u_* of 2.0 cm/s, and a kinematic viscosity ν of 0.01 cm^2/s). Figure 3 also shows the corresponding logarithmic approximation (10). For z less than about 0.25 cm the viscous correction to the logarithmic approximation is negative, and for z greater than about 2 cm the wake correction to the logarithmic approximation is positive. The logarithmic approximation (10) is accurate in less than 20% of the water column, in this example.

If the bottom is fixed and rough, instead of smooth, the wake correction is unchanged, but the wall function $f(z_+)$ must be modified to incorporate the effect of roughness. Equation (6) must be replaced by

$$\overline{u}(z) = u_* f'\left(\frac{z}{k_s}, \frac{k_s u_*}{\nu}\right) + u_* W(\xi) \tag{11}$$

where k_s is the equivalent Nikuradse sand roughness of the bottom, as before. For zu_*/ν greater than about 50 and sufficiently large z/k_s (in practice z/k_s greater than very roughly one), $f'(z/k_s, k_s u_*/\nu)$ is logarithmic:

$$f'\left(\frac{z}{k_s}, \frac{k_s u_*}{\nu}\right) \simeq \frac{1}{\kappa} ln\left(\frac{z}{k_s}\right) + B\left(\frac{k_s u_*}{\nu}\right) \tag{12}$$

where $B(k_s u_*/\nu)$ is an empirical function (Schlichting, 1979). If $k_s u_*/\nu$ is less than about 5, the bottom is hydrodynamically smooth, and equation (12) matches equation (7). If $k_s u_*/\nu$ is greater than about 70, the bottom is hydrodynamically rough, and $B(k_s u_*/\nu)$ has a constant value of about 8.5 (Schlichting, 1979).

If the bottom is rough or smooth, and we consider the region in which z/h is less than about 0.2 while z is greater than about $50\nu/u_*$ or roughly k_s (whichever is greater), we may neglect the wake correction and use equation (12) to obtain the following commonly used logarithmic approximation:

$$\overline{u}(z) \simeq \frac{u_*}{\kappa} ln\left(\frac{z}{z_o}\right). \tag{13}$$

Here z_o is the wall roughness scale, which is a function of $k_s u_*/\nu$ given by

$$z_o = k_s exp[-\kappa B(k_s u_*/\nu)]. \tag{14}$$

In principle one can use equation (13) with mean velocity measurements in the appropriate region in order to estimate the shear velocity, by regressing measurements of $\overline{u}(z)$ against $ln(z)$. This is the log profile technique for estimating the shear velocity (e.g. Grant et al. 1984).

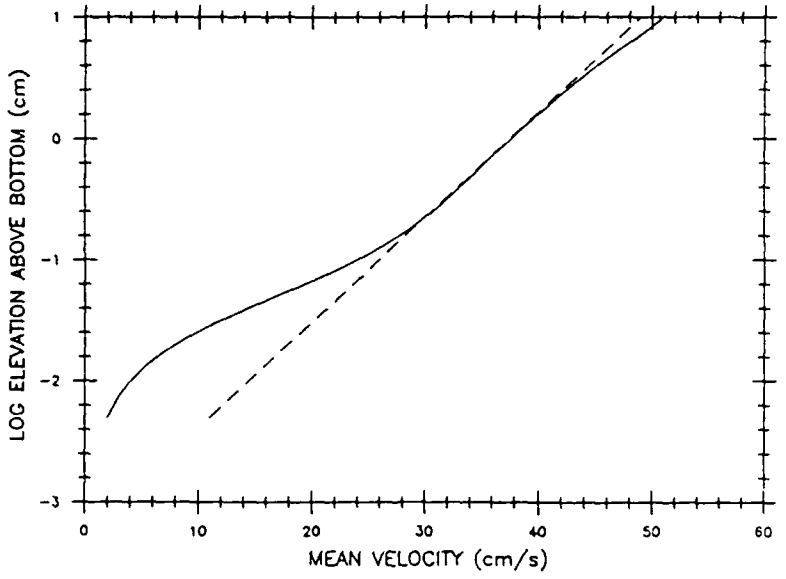

Figure 3: Velocity profile in turbulent one-dimensional open channel flow for $h = 10$ cm, $u_* = 2.0$ cm/s and $\nu = 0.01$ cm^2/s. Solid line: complete profile based on equations (6), (8) and (9). Dashed line: logarithmic approximation based on equation (10).

2.5 TURBULENCE INTENSITIES AND SPECTRA

Nezu and Rodi (1986) suggested the following empirical expressions for the root-mean-square turbulent velocity fluctuations in a one-dimensional open channel flow above a smooth bottom, for the region in which zu_*/ν is greater than about 50 and z/h is less than about 0.6:

$$\frac{(\overline{u'^2})^{1/2}}{u_*} = D_u exp(-\lambda_u \xi) \tag{15}$$

$$\frac{(\overline{w'^2})^{1/2}}{u_*} = D_w exp(-\lambda_w \xi). \tag{16}$$

Here D_u, λ_u, D_w and λ_w are empirical constants and the other symbols have the same meanings as before. Nezu and Rodi found $D_u \simeq 2.26, \lambda_u \simeq 0.88, D_w \simeq 1.23, \lambda_w \simeq 0.67$. Nezu and Rodi (1986) also suggested the following empirical expression for all z/h less than about 0.6:

$$\frac{(\overline{u'^2})^{1/2}}{u_*} = D_u exp(-\lambda_u \xi)\Gamma + 0.3 z_+ (1 - \Gamma) \tag{17}$$

where

$$\Gamma = 1 - exp\left(-\frac{z_+}{B'}\right) \tag{18}$$

They suggested that $B' \simeq 10$. Presumably equations (15) and (16) apply to rough as well as smooth walls, because these equations are normalized by the "outer" variables u_* and h. Equation (17) apparently applies only to smooth walls.

It is convenient to define the following spatial correlation functions:

$$\phi_{11}(L) = \langle u'(x,y,z,t)u'(x+L,y,z,t)\rangle \tag{19}$$

$$\phi_{33}(L) = \langle w'(x,y,z,t)w'(x+L,y,z,t)\rangle \tag{20}$$

where angular brackets denote a mean value. The corresponding wavenumber spectra are

$$\psi_{11}(k) = \frac{1}{\pi}\int_{-\infty}^{+\infty} \phi_{11}(L)e^{-ikL}dL \tag{21}$$

$$\psi_{33}(k) = \frac{1}{\pi}\int_{-\infty}^{+\infty} \phi_{33}(L)e^{-ikL}dL \tag{22}$$

The above spatial correlation functions and wavenumber spectra are of fundamental interest, but are difficult to measure directly. The more easily measurable temporal correlation functions are

$$R_{11}(T) = \langle u'(x,y,z,t)u'(x,y,z,t+T)\rangle \tag{23}$$

$$R_{33}(T) = \langle w'(x,y,z,t)w'(x,y,z,t+T)\rangle \tag{24}$$

and the corresponding frequency spectra are

$$S_{11}(\omega) = \frac{1}{\pi}\int_{-\infty}^{+\infty} R_{11}(T)e^{-i\omega T}dT \tag{25}$$

$$S_{33}(\omega) = \frac{1}{\pi}\int_{-\infty}^{+\infty} R_{33}(T)e^{-i\omega T}dT \tag{26}$$

According to Taylor's frozen turbulence hypothesis, the fluctuating component of the turbulent velocity field may for some purposes be regarded as if it were being advected along,

without changing structure, by the mean flow. An analysis based on the frozen turbulence hypothesis shows the wavenumber and frequency spectra are related by

$$\psi_{11}(k) = \overline{u}(z) S_{11}[\overline{u}(z)k] \tag{27}$$

$$\psi_{33}(k) = \overline{u}(z) S_{33}[\overline{u}(z)k] \tag{28}$$

where $\overline{u}(z)$ is the mean velocity at the elevation of interest.

According to Kolmogorov's universal equilibrium theory (see Batchelor, 1967) an inertial subrange exists in the wavenumber spectrum if the Reynolds number is sufficiently large. In the inertial subrange, the inverse wavenumber is much smaller than the scale of the energy containing eddies but much larger than the scale of the dissipative eddies, and it is reasonable to assume that the wavenumber spectrum depends only on the wavenumber and the local mean rate of energy dissipation per unit mass (ε). The following relationships then follow from dimensional analysis:

$$\psi_{11}(k) = \alpha_1 \varepsilon^{2/3} k^{-5/3} \tag{29}$$

$$\psi_{33}(k) = \alpha_3 \varepsilon^{2/3} k^{-5/3}. \tag{30}$$

Here α_1 and α_3 are empirical constants, related in principle, because of the assumed isotropy of the small-scale motion, by $\alpha_3 = (4/3)\alpha_1$. The values of the empirical constants are poorly determined at present. Grant et al. (1984) suggested $\alpha_1 \simeq 0.4$ and $\alpha_3 = (4/3)\alpha_1 \simeq 0.5$. The existence of a well-developed inertial subrange requires that the scale of the large-scale motion must be very much larger than the scale of the dissipative motions, so that $(u_* h/\nu)^{3/8}$ must be much larger than unity (Batchelor, 1967). A well developed inertial subrange often does not exist in a small-scale laboratory channel.

3 MEASUREMENTS AND DISCUSSION

The purpose of the measurement program reported here was to determine whether the 17-Meter Flume can produce a flow with the idealized characteristics described in Section 2. The measurement program consisted of three components. The first was a set of preliminary measurements designed to establish an adequate sampling scheme, to establish repeatability of measurements, and to establish approximate independence of along-stream position and cross-stream position. The second component of the measurement program was a set of vertical profiles of mean velocity, Reynolds stress and turbulence intensity at a fixed location under five different sets of flow conditions. The third component was a set of long records at a fixed point under different flow conditions, used to compute spectra and examine frequency content. All measurements were carried out above the smooth PVC false bottom, with the two-axis LDV sampling at a rate of 32 hz.

3.1 PRELIMINARY MEASUREMENTS

We carried out the preliminary measurements under a fixed set of conditions in which the water temperature was 20°C, the nominal water depth was 12 cm, and the nominal flow

speed at the water surface was 10 cm/s. The bottom slope required to drive a uniform flow over a smooth bottom under these conditions (about 2×10^{-5}, corresponding to a drop in elevation of about 0.04 cm over the entire 17-m length of the raceway) is comparable to the estimated resolution of our measurements of bottom slope, and is smaller than the slope of the irregularities in the bottom of the flume. We therefore set the bottom slope as closely as possible to zero. The flow was driven against the retarding action of boundary friction by a streamwise pressure gradient set up by a small unresolved surface slope, acting with or against a small unresolved bottom slope. Although this flow differs in detail from the idealized uniform flow considered in Section 2, a simple order-of-magnitude argument shows that the two flows are in fact essentially dynamically equivalent. At low Froude numbers the streamwise advective acceleration caused by the sloping water surface has a negligible effect on the mean momentum balance, and the streamwise pressure gradient is dynamically equivalent to a down-slope gravitational force. All of the equations given in Section 2 are unchanged, with the exception of equation (3), which must be modified to incorporate the effect of the surface slope. The required modification to equation (3) does not affect the results presented here.

Most of the preliminary measurements are profiles of mean velocity and Reynolds stress. Each profile has ten measurement points spaced unequally in the vertical direction, with the densest sampling in the region where a logarithmic velocity profile was expected. The record length at each measurement station was six minutes, so that the time required to produce a set of measurements for one profile was one hour. We chose the number of measurement points and the record length somewhat arbitrarily. The values that we used seemed to provide a reasonable compromise between the desire for good statistics and the desire to complete the measurements in a reasonable amount of time. The record length was in all cases much longer than the time scale h/U required for energetic eddies to be advected past the measurement station.

In order to test in a simple way the ability of a six-minute record to produce stable means, we took a long record of the streamwise velocity at a station 3 cm above the bottom. We then computed the running average $\hat{u}(t_*)$, defined by

$$\hat{u}(t_*) = \frac{1}{t_*} \int_0^{t_*} u(t)dt \tag{31}$$

as a function of the averaging time t_*. Figure 4 shows the results of this calculation, in the form of a departure of the running average from the mean of the total record, normalized by the mean of the total record. Figure 4 indicates fluctuations of order 2% to 3% for averaging times less than about 2000 s, and fluctuations that are an order of magnitude smaller for averaging times greater than about 2000 s. These results suggest that an averaging time of

six minutes is sufficient to produce estimates of mean velocities that are within a few percent of the true mean. Estimates of Reynolds stress based on six-minute averages probably have much larger departures from the true Reynolds stress, because the instantaneous Reynolds stress is typically more intermittent than the instantaneous streamwise velocity. In addition, the standard deviation of the instantaneous Reynolds stress is comparable to the mean Reynolds stress, while the standard deviation of the instantaneous streamwise velocity is an order of magnitude smaller than the mean streamwise velocity.

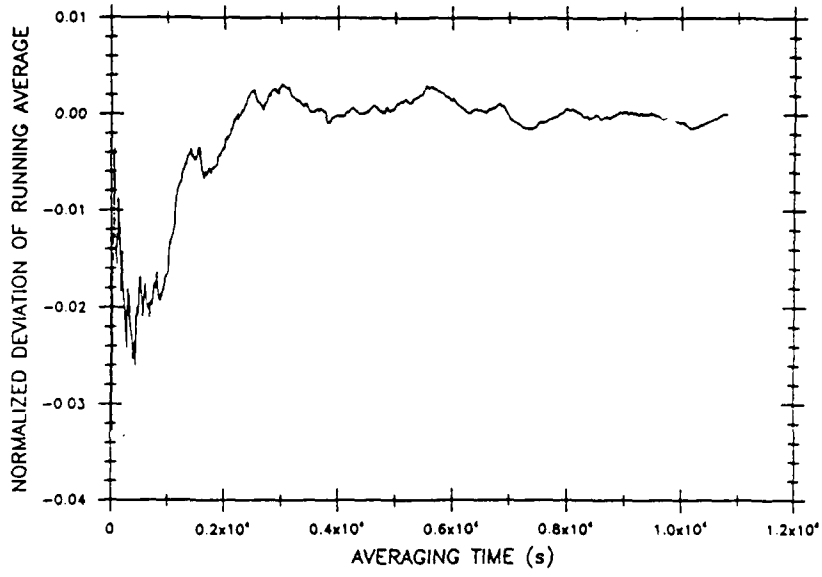

Figure 4: Running average $\hat{u}(t_*)$, defined by equation (31), as a function of averaging time t_*. The vertical axis is the departure of the running average from the mean of the total record, normalized by the mean of the total record.

Figure 5 shows three consecutive mean velocity profiles and three consecutive Reynolds stress profiles, in order to demonstrate repeatability. Both the mean velocity and the Reynolds stress have roughly the expected vertical distribution, and both are quite repeatable. As expected, the variability of the Reynolds stress estimates is much larger than the variability of the mean velocity estimates.

A

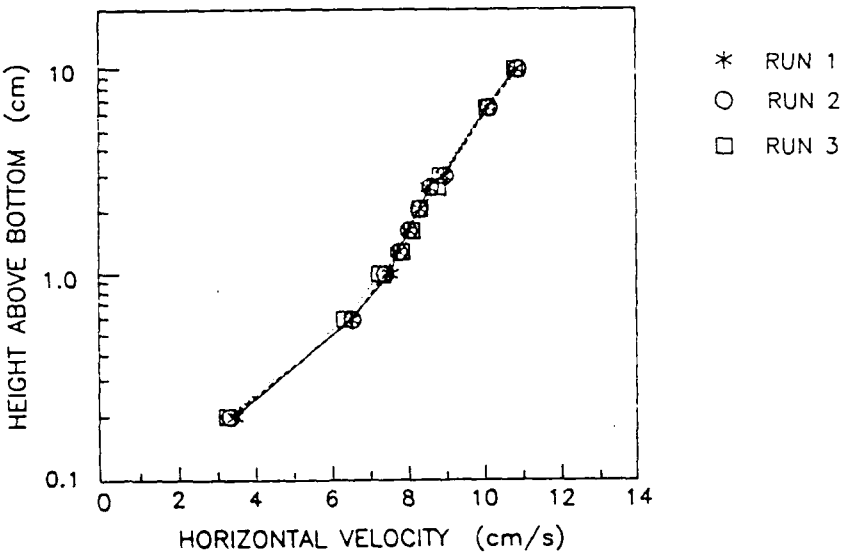

B

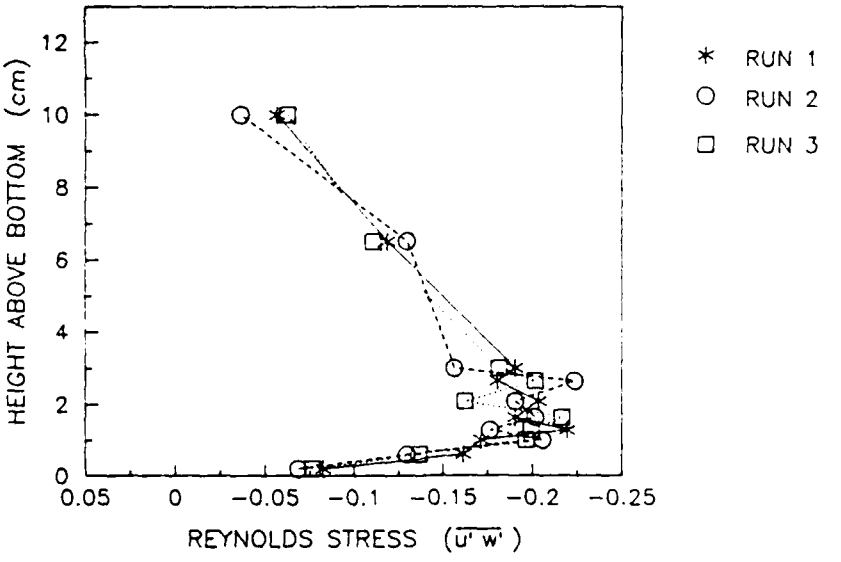

Figure 5: Consecutive profiles of the mean velocity (A) and Reynolds stress (B) in the preliminary measurement program. The measurement station was on the channel centerline, 12.8 m downstream of the channel entrance.

Mean velocity profiles obtained at the center of the channel and at various distances from the upstream end of the flume indicate that the mean velocity is fully developed within about 9.2 m or 75 water depths of the entrance, roughly as expected (see Figure 6A). The slope of the logarithmic region of the velocity profile does not change appreciably between 9.2 m and 15.6 m. The Reynolds stress profiles show a trend, however, with increasing values of stress all the way to 15.6 m (see Figure 6B). We have not identified the cause of the continuing evolution of the Reynolds stress, and we have not determined whether it is repeatable. It is possible that the Reynolds stress requires a longer entrance length than does the mean velocity.

Velocity profiles and stress profiles at different cross-stream positions in 5-cm intervals from the flume centerline indicate that the central 20 cm of the flow can be considered independent of cross-stream position (see Figure 7), in rough agreement with Nakagawa's formula (see Section 2). It is interesting to note in Figure 7 that the near-surface stress close to the side walls changes sign, and that there is a corresponding sign change in the velocity gradient $d\overline{u}/dz$.

3.2 PROFILES OF MEAN VELOCITY, REYNOLDS STRESS AND TURBULENCE INTENSITY

We chose five flow regimes at a fixed nominal depth of 12 cm and nominal surface speeds of 10, 20, 30, 40 and 50 cm/s in order to investigate in detail the vertical structure of mean velocity, Reynolds stress and turbulence intensity. The flume settings used to achieve these regimes are given by Butman and Chapman (1989). In all cases the measurement station was on the centerline of the flume at a position 12.8 m from the upstream end. Each vertical profile had ten measurement stations and the record length at each station was six minutes, as in the preliminary measurements. Table 1 shows the actual depth, water temperature and bottom slope for each case. We set the bottom slope of the flume as closely as possible to an *a priori* estimate of the value required to drive the flow in a one-dimensional state. We did not carry out detailed measurements of the water depth as a function of position, and we therefore do not know whether the water surface was in fact parallel to the bottom. Order-of-magnitude estimates indicate, however, that the small departures from one-dimensional flow that probably occurred had a small effect on the mean momentum balance, so that the flows were approximately the same as the idealized flow discussed in Section 2. As stated in Section 3.1, all of the equations presented in Section 2 are unchanged by the small departures from a one-dimensional state, with the exception of equation (3). The required modification to equation (3) does not affect the results presented here.

In our analysis of the velocity measurements, we rotated the coordinate system at each point so that the z-component of the mean velocity was zero. Use of a different rotation angle at each elevation is not quite consistent (see Section 3.2.2) but the required rotations were small in all cases, and the effect of the rotation had very little quantitative and no qualitative effect.

A

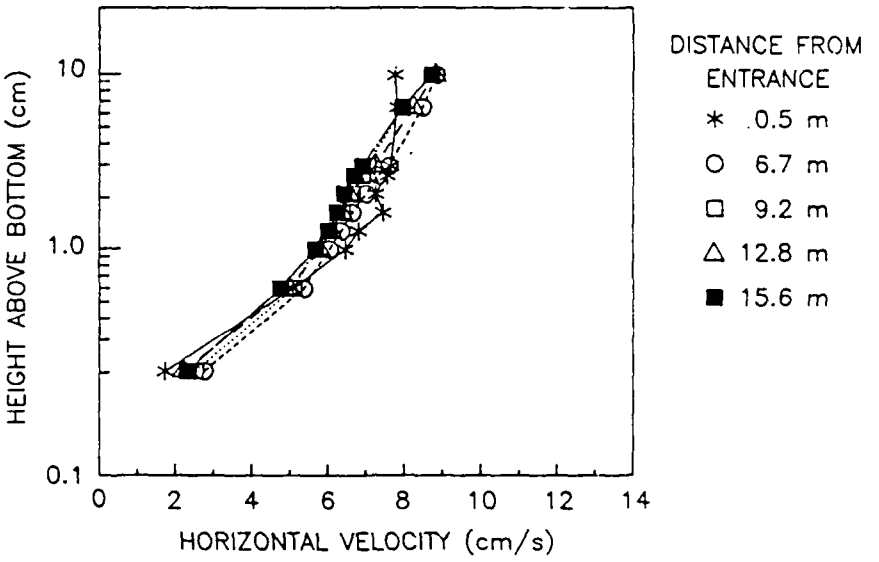

B

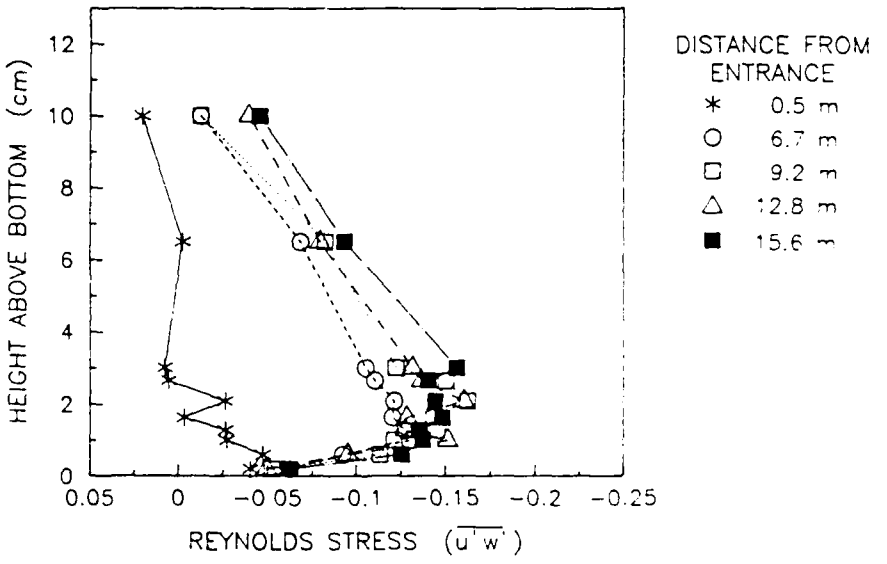

Figure 6: Profiles of mean velocity (A) and Reynolds stress (B) at various distances along the channel, obtained in the preliminary measurement program. All measurements were taken along the centerline.

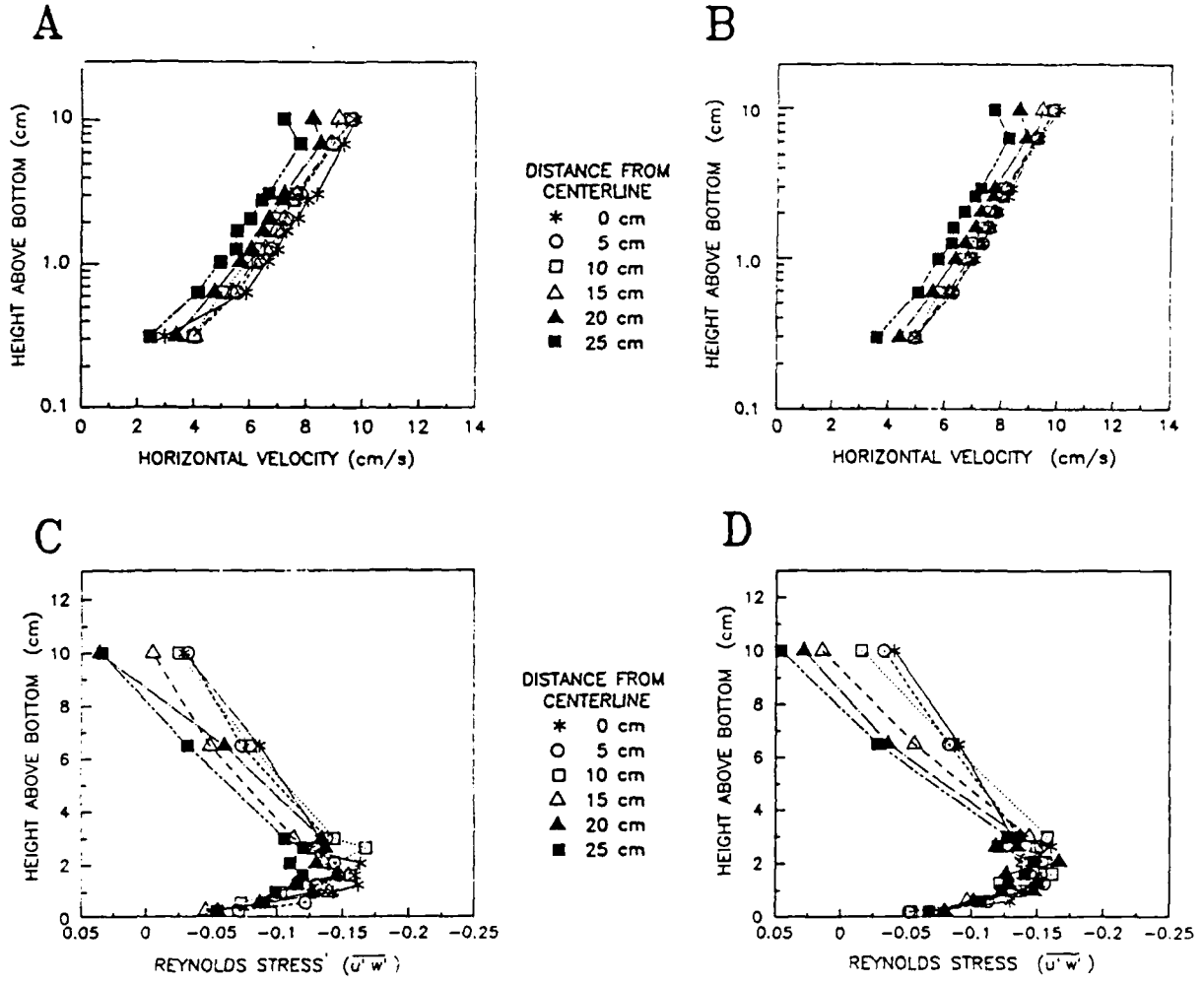

Figure 7: Profiles of mean velocity (A and B) and Reynolds stress (C and D) as a function of cross-channel position, obtained in the preliminary measurement program. Looking downstream, the profiles shown in A and C were taken from the centerline moving toward the right-hand wall, and the profiles shown in B and D were taken from the centerline moving toward the left-hand wall. All measurements were taken 12.8 m downstream of the channel entrance.

Table 1: Test Conditions for Velocity, Stress and Intensity Profiles.

Test	Depth at Measurement Station (cm)	Nominal Flow Speed (cm s^{-1})	Bottom Slope	Water Temperature (°C)
1	12.1	10	0.00	7.6
2	11.3	20	1.15×10^{-4}	20
3	11.5	30	2.69×10^{-4}	20
4	11.6	40	4.62×10^{-4}	20
5	11.4	50	7.31×10^{-4}	20

3.2.1 Initial Analysis of Mean Velocity and Reynolds Stress

In our initial analysis of Reynolds stress profiles, we used only the measurements well outside of the viscous region near the bottom ($z > 50\nu/u_*$) and we obtained an estimate of the bottom stress τ_b for each elevation by using equation (5). We then computed the mean of the estimates of τ_b for all elevations, divided the mean by the density, and took the square root of the resulting value to obtain an estimate of the shear velocity. We determined corresponding 95% confidence intervals by linearizing the estimation problem (e.g. Draper and Smith, 1966), and assuming normally distributed, uncorrelated residuals. We call this method for estimating the shear velocity the "Reynolds stress technique."

In our initial analysis of mean velocity profiles, we used only the measurements in the region where a logarithmic profile was expected ($50\nu/u_* < z < 0.2h$), and we regressed the mean velocity against $ln(z)$ in order to estimate the shear velocity (see equation [10]). We used standard estimation techniques (e.g. Draper and Smith, 1966) to determine corresponding 95% confidence intervals. We call this method for estimating the shear velocity the "log profile technique."

Table 2 shows estimates of the shear velocity based on the log profile technique and the Reynolds stress technique, with corresponding 95% confidence intervals, normalized correlation coefficients (r^2), and number of measurements used in the estimate (N). Although the regressions produced reasonably good fits to the measurements (indicated by fairly high values of r^2), estimates of shear velocity based on the log profile technique were consistently larger than estimates based on the Reynolds stress technique in Tests 2 through 5, and the two estimates were not consistent in Tests 2 and 4. We are not sure why these discrepancies occurred. A possible contributing factor was neglect of viscous effects and the wake correction in the log profile technique. A second possible contributing factor was the presence of velocity fluctuations at very low frequencies (see Section 3.3), which may have caused estimates of mean velocity and Reynolds stress based on six-minute averages to have relatively large errors, and may have caused errors at different points in the profiles to be correlated with each other. A third possible contributing factor was the small vertical extent of the region in which a logarithmic mean velocity profile was expected (typically 1 to 2 cm).

Table 2: Initial Estimates of Shear Velocity.

	Log profile technique			Reynolds-stress technique	
Test	u_* (cm/s)	r^2	N	u_* (cm/s)	N
1	0.49		2	0.50 ± 0.04	6
2	1.06 ± 0.15	0.991	5	0.81 ± 0.06	9
3	1.48 ± 0.28	0.984	5	1.20 ± 0.13	9
4	1.94 ± 0.15	0.997	5	1.56 ± 0.17	9
5	2.32 ± 0.19	0.997	5	2.00 ± 0.21	9

3.2.2 Detailed Analysis of Mean Velocity and Reynolds Stress

In order to resolve the differences between estimates of shear velocity based on the log profile technique and the Reynolds stress technique, we used a slightly more sophisticated analysis of the mean velocity profile, in which we fit mean velocity measurements in the entire water column to equation (6) in Section 2.4, with the wall function $f(z_+)$ and the wake correction $W(\xi)$ given by equations (8) and (9), respectively. Because we were not sure that the origin of the measurement system coincided with the true bottom of the flume, we replaced the vertical coordinate z in equation (6) by the quantity z', defined by

$$z' = z + \Delta. \tag{32}$$

Here Δ is the displacement of the true bottom of the flume below the origin of the measurement system. We fit equation (6) to the measured mean velocity profiles by least-squares regression, using the shear velocity u_*, the Coles parameter Π and the displacement Δ as fitting parameters. We used the Coles parameter as a fitting parameter because its value is not well established for open-channel flow, and because Nezu and Rodi (1986) found that it may depend on Reynolds number. We solved the nonlinear regression problem by using an iterative technique in which one linearizes the problem about estimates of the parameters, and then solves the linearized problem repeatedly, updating the parameter estimates at each iteration. We estimated variances and confidence intervals for the parameters by linearizing the regression problem about the final values of the parameter estimates. We call this method for estimating the shear velocity, the Coles parameter and the displacement Δ the "velocity profile technique."

Table 3 shows estimates based on the velocity profile technique, with corresponding 95% confidence intervals. The values of the kinematic viscosity ν indicated in the table were determined as a function of temperature by using a formula given by White (1979). The estimates of shear velocity in Table 3 are consistent with estimates based on the Reynolds stress technique (see Table 2). The estimates of the displacement Δ are consistent with expectations, although the confidence intervals are in most cases large enough so that estimates of Δ do not differ significantly from zero. The relatively large value of Δ in Test 4 may indicate an operator error in which the LDV was positioned incorrectly. The estimates of the Coles parameter Π shown in Table 3 are consistent in magnitude with the values found by Nezu and Rodi (1986), although we do not find a consistent increase with Reynolds number, as they

did. The confidence intervals are possibly large enough to obscure a consistent dependence on Reynolds number.

Table 3: Results of Velocity Profile Technique.

Test	ν (cm^2/s)	u_* (cm/s)	Δ (cm)	Π
1	0.0142	0.51 $\pm$ 0.01	0.01 $\pm$ 0.03	0.20 $\pm$ 0.15
2	0.0102	0.87 $\pm$ 0.01	-0.05 $\pm$ 0.03	0.27 $\pm$ 0.09
3	0.0102	1.21 $\pm$ 0.02	-0.01 $\pm$ 0.03	0.37 $\pm$ 0.15
4	0.0102	1.58 $\pm$ 0.01	-0.11 $\pm$ 0.02	0.26 $\pm$ 0.10
5	0.0102	1.99 $\pm$ 0.03	-0.01 $\pm$ 0.04	0.27 $\pm$ 0.14

Figure 8 shows an example of a measured mean velocity profile and a fitted curve based on equation (6) for Test 4 (with a nominal flow speed of 40 cm/s). Figure 9 shows mean velocity measurements for all five tests in wall coordinates ($\overline{u}(z)/u_*$ as a function of zu_*/ν) together with the velocity profile given by equations (6) and (8) without the wake correction. The wake correction is not included in the semi-empirical curve in Figure 9 because the wake correction is different for each test, so that a single line would not represent all of the tests. The measurements in Figure 9 diverge from the semi-empirical curve at large z, as expected. The measurements collapse very well onto the semi-empirical curve in the wall region.

To compare the above results with measurements of Reynolds stress, we constructed semi-empirical curves for the Reynolds stress by combining the estimates of u_*, Π and Δ given in Table 3 with equation (4), using equations (6), (8) and (9) to determine the mean velocity gradient $d\overline{u}/dz$. Curves constructed in this manner compare quite well with measurements of Reynolds stress, especially at lower flow speeds (see Figure 10). At higher flow speeds, the calculated semi-empirical values are larger than the measured Reynolds stresses in the thin viscous sublayer very near the bottom, and the measured Reynolds stress at the lowest measurement point in fact changes sign (see Figure 11).

We are not sure why the measured Reynolds stress departs from the calculated Reynolds stress very near the bottom, or why the Reynolds stress very near the bottom changes sign at higher flow speeds. A possible explanation is interference of the bottom with the light beams from the laser. A second possible explanation is the potential presence of weak secondary mean flows in the y and z directions, which may transfer x momentum vertically, and may therefore change the turbulent transfer of momentum by the Reynolds stress.

Our measurements of the z component of the mean velocity suggest inconclusively that weak secondary mean motions may be present. In an idealized one-dimensional channel flow, the z component of the mean velocity is zero. Measurements of the z component of the mean velocity may be nonzero because of a small rotation of the measurement system with respect to the mean flow direction. If this is the case, the ratio of the z component to the x component of the mean velocity should be independent of z. In contrast, our

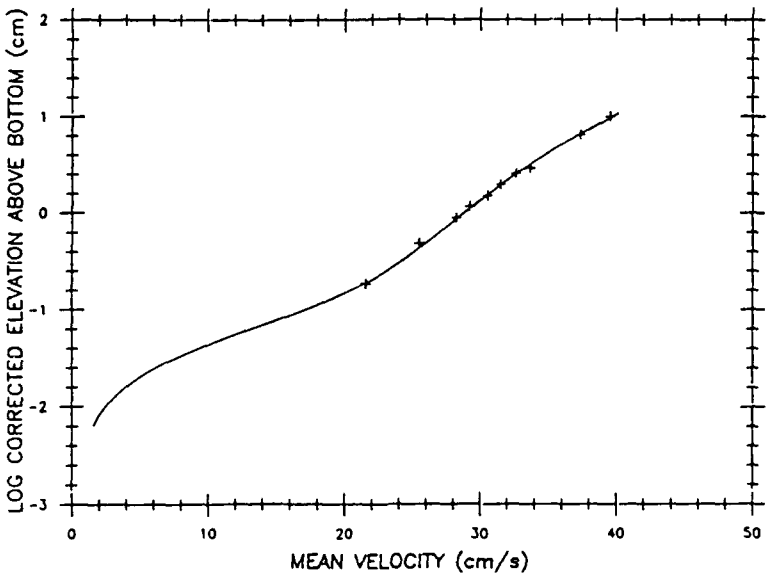

Figure 8: Mean velocity profile in Test 4 (see Table 1). Crosses: measurements. Solid line: curve fit by velocity profile technique.

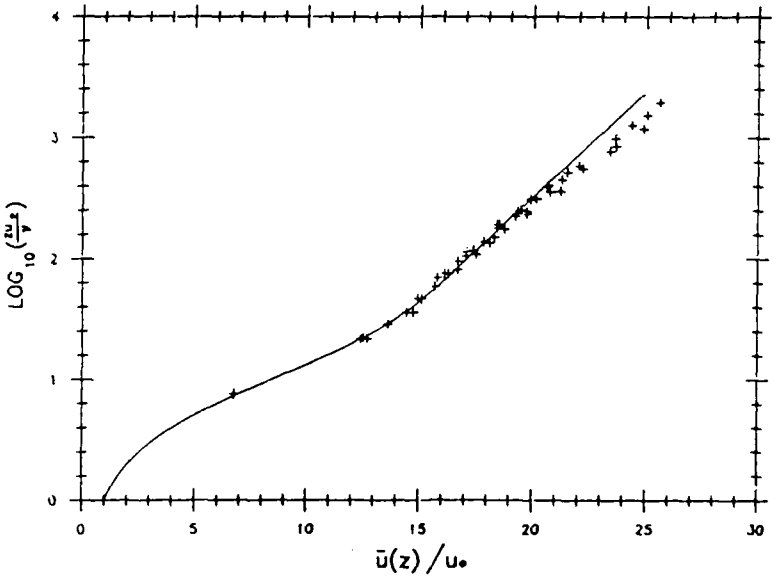

Figure 9: Mean velocities in Tests 1 through 5 (see Table 1). Crosses: measurements. Solid line: semi-empirical expression based on equations (6) and (8), without the wake correction.

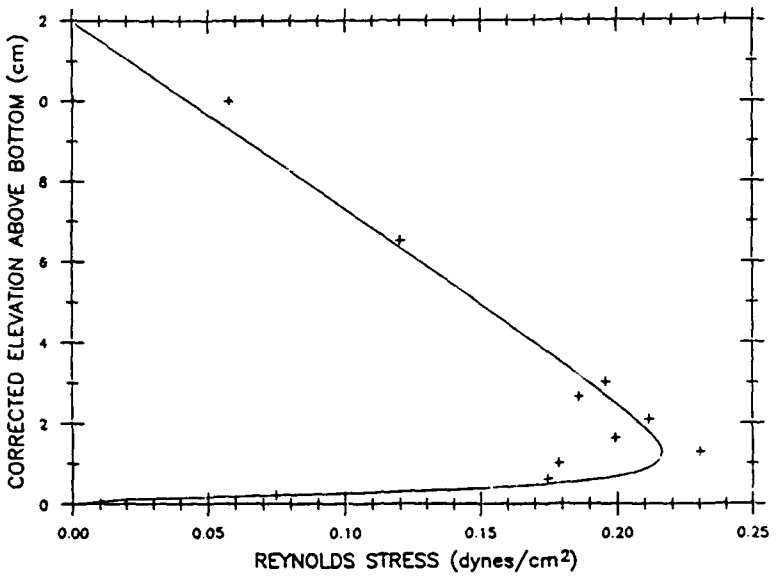

Figure 10: Reynolds stress profile in Test 1 (see Table 1). Crosses: measurements. Solid line: equation (4), with $d\overline{u}/dz$ given by equations (6), (8) and (9), and u_*, Π and Δ given in Table 3.

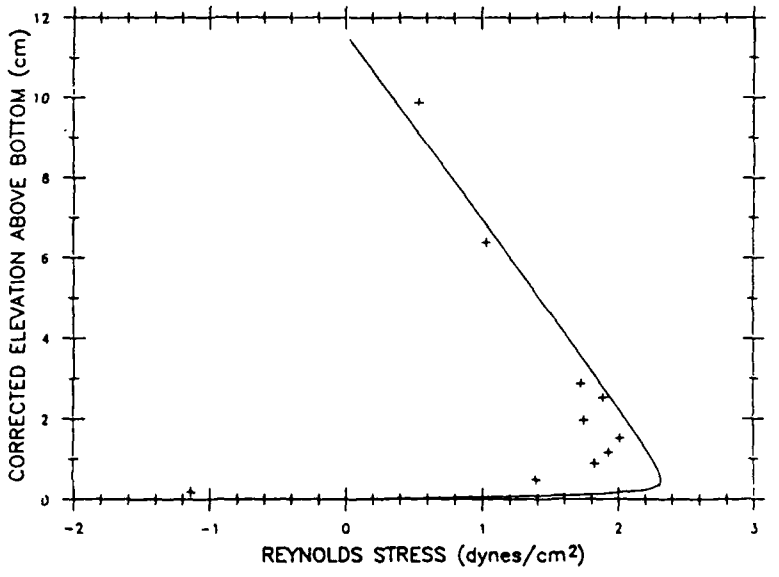

Figure 11: Reynolds stress profile in Test 4 (see Table 1). Crosses: measurements. Solid line: equation (4), with $d\overline{u}/dz$ given by equations (6), (8) and (9), and u_*, Π and Δ given in Table 3.

measurements show that the ratio of the z component to the x component of the mean velocity has a nonuniform vertical structure, with a relatively large negative value very near the bottom at the centerline, and weaker positive values higher up in the water column (see Figure 12). We find this structure at all flow speeds. This structure develops in a consistent manner in x, from the upstream end of the channel to the measurement station, and it varies in y. Although clearly not conclusive, these measurements suggest the possible presence of secondary flows. The measurements of Nezu and Rodi (1986) are insufficient to address this question in detail, because they did not measure the z component of the velocity at points lower than 14 mm above the bottom, and we see the clearest evidence of mean vertical flows at locations well below this point.

3.2.3 Turbulence Intensities

Our measurements of turbulence intensities compare very well with the empirical expressions suggested by Nezu and Rodi (1986). For example, Figure 13 shows a comparison of equation (17) and our measurements of $< u'^2 >$ in Test 1. The agreement between the empirical expression and the measurements is comparable to that obtained by Nezu and Rodi (1986). Figure 14 shows a comparison of equation (16) and our measurements of $< w'^2 >$ in all five tests. Again, the agreement is comparable to that obtained by Nezu and Rodi (1986). In Figure 14, the departure of the empirical curve from the measurements very near the bottom is due to the fact that the empirical expression is valid only well outside of the viscous sublayer.

3.3 SPECTRA

We carried out a brief investigation of spectra in order to determine whether the measured spectra were consistent with the idealized spectra described in Section 3, and why we required record lengths much longer than the time scale h/U in order to obtain accurate estimates of mean velocities (see Figure 4). To investigate spectra, we used a half-hour record obtained at an elevation of 3 cm above the bottom in a flow with a depth of 10 cm, a nominal speed of 10 cm/s and a water temperature of 20°C. The mean velocity at the measurement point was 8.4 cm/s and the shear velocity was about 0.47 cm/s. We also examined velocity records obtained under other flow conditions, and found the same qualitative features described here.

Figures 15 and 16 show wavenumber spectra of the horizontal and vertical velocity fluctuations, computed from frequency spectra by using the frozen turbulence hypothesis (see Section 2.5). Figures 15 and 16 also show theoretical curves for the inertial subrange, calculated from equations (29) and (30). The spectra show several interesting features.

At high wavenumbers, the spectral density is nearly constant, possibly reflecting aliasing, a noise floor, or both. The vertical velocity spectrum shows well defined spikes at high frequencies. The highest spike occurs at a frequency of about 6 hz, and the second-highest

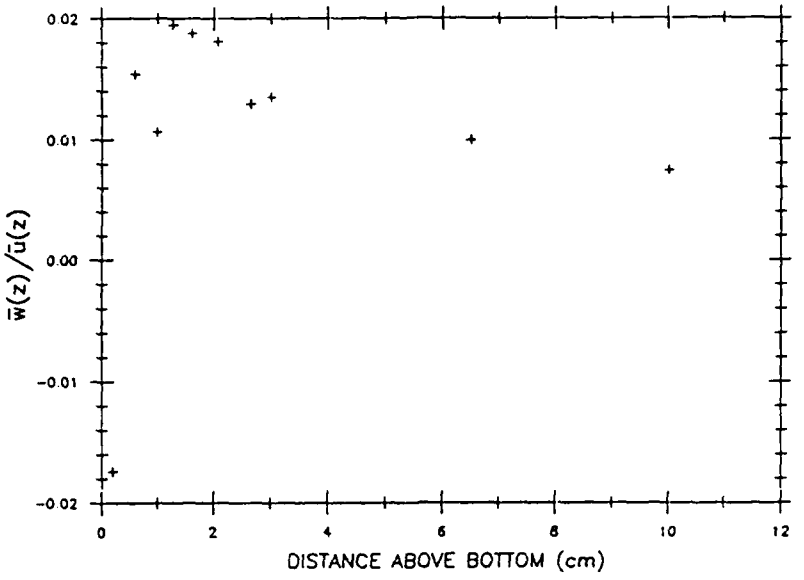

Figure 12: Ratio of z-component of mean velocity to x-component of mean velocity as a function of elevation in Test 1 (see Table 1)

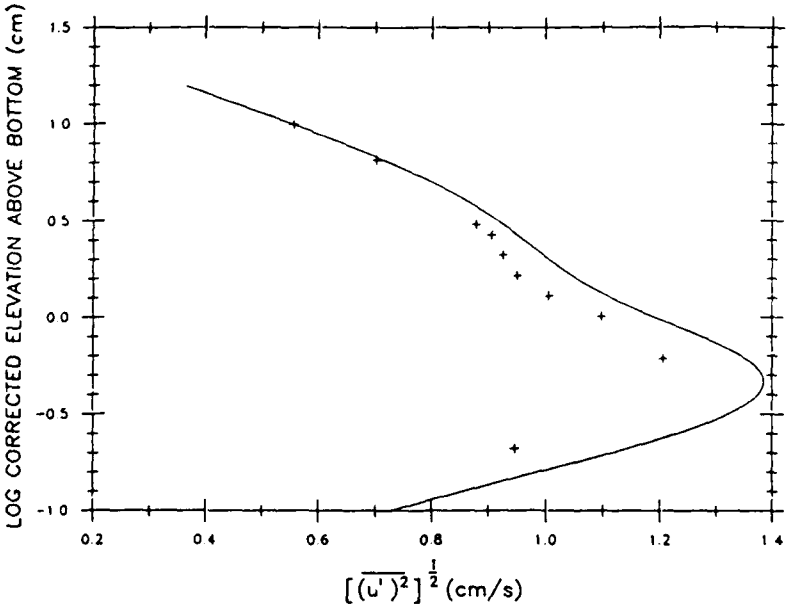

Figure 13: Turbulence intensity $(\overline{u'^2})^{1/2}$ in Test 1 (see Table 1). Crosses: measurements. Solid line: equation (17) with u_* and Δ given in Table 3.

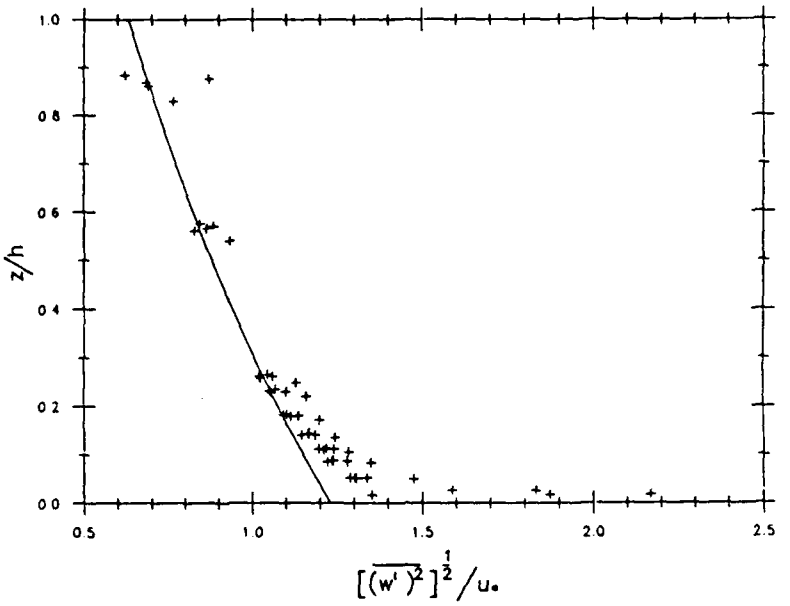

Figure 14: Turbulence intensity $(\overline{w'^2})^{1/2}$ in all five tests (see Table 1). Crosses: measurements normalized by u_* given in Table 3. Solid line: equation (16).

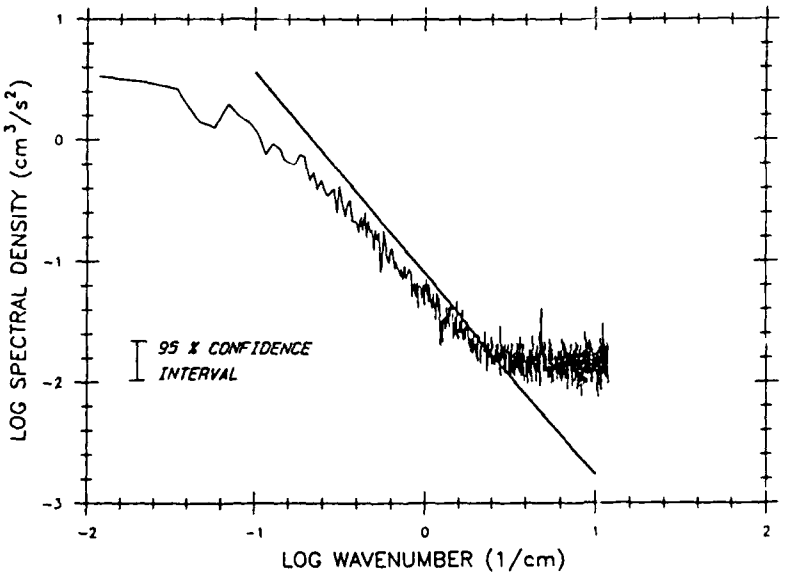

Figure 15: Wavenumber spectrum of horizontal velocity fluctuations. Solid line: measurements. Heavy line: equation (29) with $\epsilon \simeq u_*^3/(\kappa z)$, $u_* = 0.47$ cm/s, $z = 3.0$ cm, $\kappa = 0.40$, and $\alpha_1 = 0.4$.

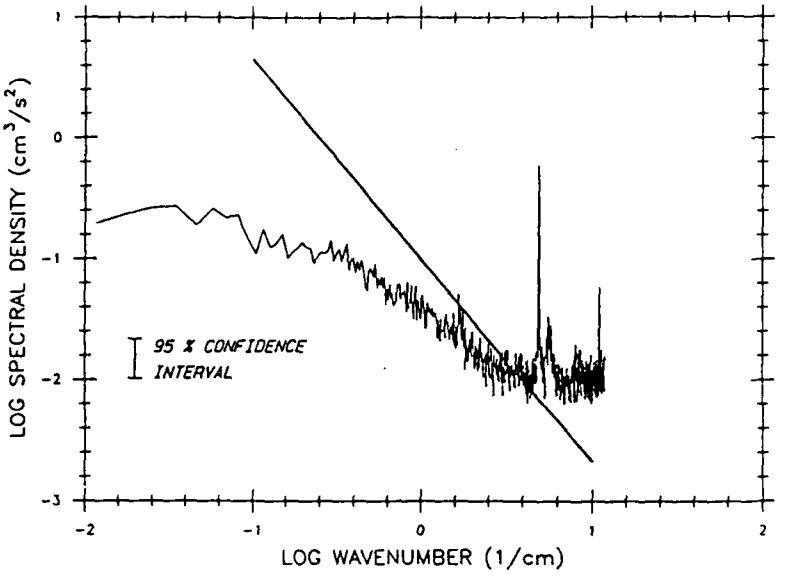

Figure 16: Wavenumber spectrum of vertical velocity fluctuations. Solid line: measurements. Heavy line: equation (30) with $\varepsilon \simeq u_*^3/(\kappa z)$, $u_* = 0.47$ cm/s, $z = 3.0$ cm, $\kappa = 0.40$, and $\alpha_3 = 0.5$.

spike occurs at a frequency of about 12 hz. These spikes may be due to vibration of the probe support (observed visually to have a natural frequency of several hertz), or some other cause. The horizontal velocity spectrum shows a somewhat surprising amount of energy at relatively low wavenumbers. The spectrum does not show a tendency to decrease with decreasing wavenumber, even at the lowest resolved wavenumber, which corresponds to a wavelength of about 600 cm and a "period" of about 70 s. These values are much longer than the spatial scale h and the time scale h/U that characterize the energetic eddies.

The theoretical curves for the inertial subrange are close to the measurements at high wavenumbers in the horizontal velocity spectrum, and somewhat further away from the measurements in the vertical velocity spectrum. We did not expect to find a well developed inertial subrange because of the relatively low Reynolds number hu_*/ν. The fact that the theoretical curves in Figures 15 and 16 are not completely consistent with the measurements is therefore not disturbing. On the other hand, the fact that the theoretical curves are somewhat consistent with the measurements is reassuring.

In order to examine low-frequency fluctuations in a slightly different way, we filtered the horizontal velocity record in the time domain, by using a simple nonrecursive digital filter with a symmetrical, triangular impulse response function. We chose this filter because of simplicity and reasonably good frequency response characteristics. This filter removes energy at frequencies higher than very roughly the inverse of the half-width of the filter.

Figure 17 shows the filtered horizontal velocity record, with a filter half-width of 8 s. The filtered record indicates fairly energetic fluctuations with time scales of about 30 s. This result is interesting, because the lowest surface mode in the flume at a depth of 10 cm has a period of roughly 30 s. Standing surface waves with small amplitudes could account for the velocity fluctuations shown in Figure 17. The wavenumber spectrum (Figure 15) does not have a peak at the wavenumber corresponding to a period of 30 s, which is about 0.025 cm^{-1}, possibly because of poor spectral resolution.

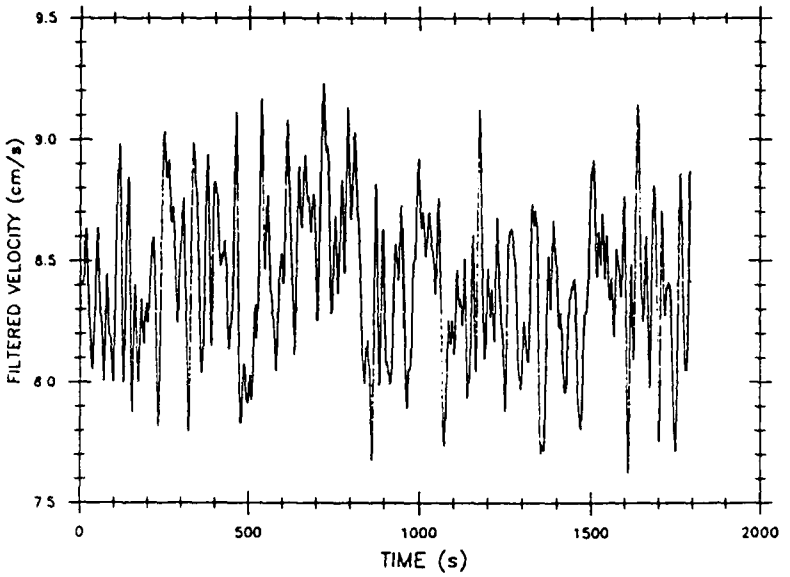

Figure 17: Filtered velocity record. Filter half width 8 s.

Figure 18 shows the filtered horizontal velocity record, with a filter half-width of 128 s. Surprisingly, this record shows fairly energetic, irregular fluctuations with time scales of several minutes. We have not identified the cause of these low-frequency fluctuations, but we think that they may have been caused by small fluctuations in pump performance, possibly due to fluctuations in the power supplied to the pump, or fluctuations due to the mechanical behavior of the pump itself. We do not think that these fluctuations were caused by surges in pump output caused by operation in a range in which the head-discharge curve for the pump has positive slope (e.g. White, 1979). According to the information that we have, the pump was operating in a range in which the slope of the head-discharge curve was negative. We also do not think that the low-frequency fluctuations were caused by instability in the hydraulic system as a whole (flume, pump, return pipe, bypass pipe and settling basins), because a simplified linear stability analysis shows that the system should have been linearly stable. Conversations with the president of a pump-manufacturing firm confirmed that the problem is likely due to fluctuations in delivery of water by the pump. He further indicated that any reasonably priced, large-volume pump able to circulate sediment slurries would probably show similar fluctuations. It should be noted that while the fluctuations shown in Figure 18 are a significant fraction of the shear velocity, they are a very small fraction of the mean velocity. This performance is probably excellent by almost any industrial standard.

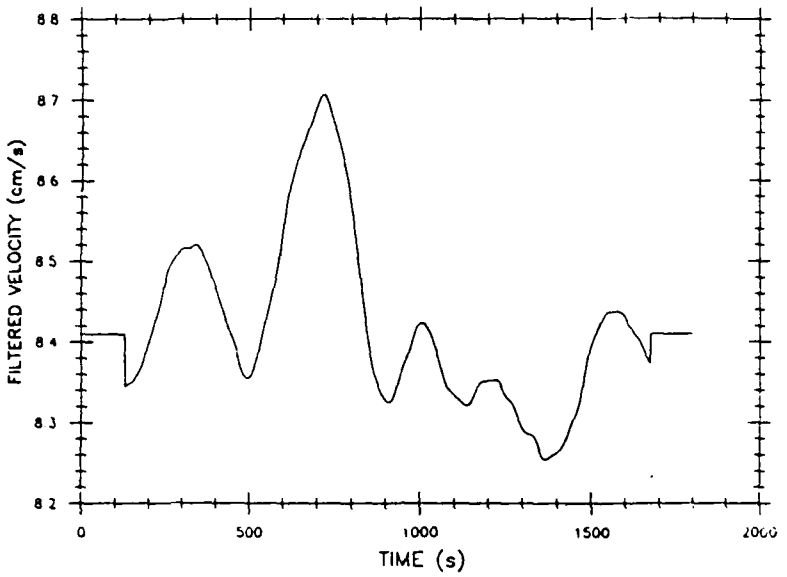

Figure 18: Filtered velocity record. Filter half width 128 s.

Straightforward order-of-magnitude arguments show that the low-frequency velocity fluctuations described here have a negligible effect on the mean momentum balance in the flume, and are therefore not important in determining the dynamics of the mean motion. This result is confirmed by the reasonably good agreement between our expectations based on previous results, and our measurements of mean velocities, Reynolds stresses and turbulence intensities. The presence of low-frequency fluctuations may explain, however, why relatively long records are required in order to obtain accurate estimates of mean values. In addition, unwanted fluctuations at low frequencies may be important if one is interested in studying the fluctuating component, in addition to the mean component, of turbulent channel flow.

4 SUMMARY AND CONCLUSIONS

In this report, we have summarized some of the important properties of one-dimensional turbulent flow in an open channel, based on existing theoretical analyses and previous laboratory measurements (Section 2). In addition, we have reported a measurement program in the 17-Meter Flume, designed to determine the extent to which vertical profiles of mean velocity and Reynolds stress are independent of along-channel and cross-channel position, and the extent to which measurements of mean velocity, Reynolds stress, turbulence intensity and spectra are consistent with expectations based on theoretical analyses and previous measurements (Section 3).

The 17-Meter Flume appears to be able to produce a flow that is approximately one-dimensional, in which the mean velocity, Reynolds stress and turbulence intensity have approximately the expected structure. The LDV as currently configured seems to be able to produce accurate measurements of mean velocity, Reynolds stress and turbulence intensity.

Unexpected oscillations with time scales of order 30 s are present in the velocity records. These oscillations may have been caused by small-amplitude standing surface waves. They do not seem to have an important effect on mean quantities and low-order statistics, but they may be important if the low-frequency part of the spectrum is of particular interest in some application. It may be possible to reduce these oscillations by redesigning the weir at the downstream end of the raceway.

Unexpected fluctuations at low frequencies (time scales of several minutes) are present in the flume, and may be caused by fluctuations in pump performance. These low-frequency fluctuations do not seem to have an important effect on mean quantities and low-order statistics, except for the fact that record lengths somewhat longer than expected may be required in order to obtain accurate estimates of means. The low-frequency fluctuations may, however, be important if the low-frequency part of the turbulence spectrum is of particular interest in some application. It may be possible to eliminate low-frequency fluctuations in the flume by installing a head tank, which could be designed to insulate the flow hydraulically from fluctuations in pump performance.

Fluctuations at well-defined high frequencies of order 10 hz (possibly associated with structural vibrations) are present in the velocity records. The well-defined spectral peaks that we find may in fact be aliased from higher frequencies. Measurements at higher sampling rates suggest well-defined spectral peaks at a frequency of about 30 hz (personal communication, Y.C. Agrawal, Flow Research, Incorporated, Kent, Washington). These high-frequency fluctuations do not seem to have an important effect on mean quantities and low-order statistics. They may be important, however, if the high-frequency part of the turbulence spectrum is of interest.

The LDV currently samples at a rate that is too slow for an accurate examination of the high-frequency part of the turbulence spectrum, and the resolution of the analog-to-digital conversion may be too coarse for some applications. These problems could be overcome in part by increasing the sampling rate to 512 hz, which is possible in principle.

5 ACKNOWLEDGEMENTS

We thank Charlotte Fuller for help with various aspects of this study, Dave Aubrey for carefully reviewing the manuscript and Shirley Bowman for typing the manuscript. Funding was provided by NOAA's National Sea Grant College Program Office, Department of Commerce (Grant No. NA86AA-D-FG090, WHOI Project No. R/O-5 to Trowbridge and Grant No. NA86-AA-D-SG090, WHOI Project No. R/P-26 to Butman), the Minerals Management Service (U.S. Department of the Interior, Contract No. 14-12-0001-30262), the

Office of Naval Research Young Investigator Program (Contract No. N00014-86-K-0579) and WHOI's Coastal Research Center (grants from Carnegie-Melon and Mobil Foundation). The U.S Government is authorized to produce and distribute reprints for government purposes notwithstanding any copyright notation that may appear hereon.

6 LITERATURE CITED

Agrawal, Y.C. and C.J. Belting. 1988. Laser velocimetry for benthic sediment transport. *Deep-Sea Res.* 35: 1047-1067.

Batchelor, G.K. 1967. *The Theory of Homogeneous Turbulence.* Cambridge University Press, London.

Butman, C.A. and R.J. Chapman. 1989. The 17-Meter Flume at the Coastal Research Laboratory. Part I: Description and User's Manual. *W.H.O.I. Tech. Rept. 89-10. CRC Rept. 89-2*, 31 pp.

Clauser, F.H. 1956. The turbulent boundary layer. *Adv. Appl. Mech.* 4: 1-51.

Coles, D. 1956. The law of the wake in the turbulent boundary layer. *J. Fluid Mech.* 1: 191-226.

Draper, N.R. and H. Smith. 1966. *Applied Linear Regression.* John Wiley and Sons.

Grant, W.D., A.J. Williams, III and S.M. Glenn. 1984. Bottom stress estimates and their prediction on the northern California continental shelf during CODE-1: The importance of wave-current interaction. *J. Phys. Oceanogr.* 14: 506-527.

Henderson, F.M. 1966. *Open Channel Flow.* MacMillan, New York.

Hinze, J.O. 1975. *Turbulence.* McGraw-Hill, New York

Komar, P.D. 1976. Boundary layer flow under steady unidirectional currents. In: D.J. Stanley and D.J.P. Swift, *Marine Sediment Transport and Environmental Management.* pp. 91-106. John Wiley & Sons, N.Y.

Landahl, M.T. 1967. A wave-guide model for turbulent shear flow. *J. Fluid Mech.* 29: 441-459.

Millikan, C.B. 1939. A critical discussion of turbulent flow in channels and pipes. *Proc. Fifth Int. Congress Appl. Mech.* (Cambridge, Massachusetts, 1938) Wiley, New York, pp. 386-392.

Monin, A.S. and A.M. Yaglom. 1971. *Statistical Fluid Mechanics.* MIT Press, Cambridge, Massachusetts.

Nakagawa, H., I. Nezu and A. Tominaga. 1983. Secondary currents in straight channel flow and the relation to its aspect ratio. *Fourth Symposium on Turbulent Shear Flows*, Karlsruhe, Fed. Rep. Germany, pp. 3.8-3.18

Nezu, I. and W. Rodi. 1986. Open channel flow measurements with a laser Doppler anemometer. *J. Hydraulic Eng.* 112: 335-355.

Nowell, A.R.M. and P.A. Jumars. 1987. Flumes: Theoretical and experimental considerations for simulation of benthic environments. *Oceanogr. Mar. Biol. Ann. Rev.* 25: 91-112.

Schlichting, H. 1979. *Boundary-Layer Theory*, 7th ed. McGraw-Hill, N.Y. 817 pp.

Tennekes, H. and J.L. Lumley. 1972. *A First Course in Turbulence*. MIT Press, Cambridge, Massachusetts.

White, F.M. 1979. *Fluid Mechanics*. McGraw-Hill, New York.

DOCUMENT LIBRARY

May 5, 1989

Distribution List for Technical Report Exchange

Attn: Stella Sanchez-Wade
Documents Section
Scripps Institution of Oceanography
Library, Mail Code C-075C
La Jolla, CA 92093

Hancock Library of Biology &
Oceanography
Alan Hancock Laboratory
University of Southern California
University Park
Los Angeles, CA 90089-0371

Gifts & Exchanges
Library
Bedford Institute of Oceanography
P.O. Box 1006
Dartmouth, NS, B2Y 4A2, CANADA

Office of the International
Ice Patrol
c/o Coast Guard R & D Center
Avery Point
Groton, CT 06340

Library
Physical Oceanographic Laboratory
Nova University
8000 N. Ocean Drive
Dania, FL 33304

NOAA/NESDIS Miami Library Center
4301 Rickenbacker Causeway
Miami, FL 33149

Library
Skidaway Institute of Oceanography
P.O. Box 13687
Savannah, GA 31416

Institute of Geophysics
University of Hawaii
Library Room 252
2525 Correa Road
Honolulu, HI 96822

Library
Chesapeake Bay Institute
4800 Atwell Road
Shady Side, MD 20876

MIT Libraries
Serial Journal Room 14E-210
Cambridge, MA 02139

Director, Ralph M. Parsons Laboratory
Room 48-311
MIT
Cambridge, MA 02139

Marine Resources Information Center
Building E38-320
MIT
Cambridge, MA 02139

Library
Lamont-Doherty Geological
Observatory
Colombia University
Palisades, NY 10964

Library
Serials Department
Oregon State University
Corvallis, OR 97331

Pell Marine Science Library
University of Rhode Island
Narragansett Bay Campus
Narragansett, RI 02882

Working Collection
Texas A&M University
Dept. of Oceanography
College Station, TX 77843

Library
Virginia Institute of Marine Science
Gloucester Point, VA 23062

Fisheries-Oceanography Library
151 Oceanography Teaching Bldg.
University of Washington
Seattle, WA 98195

Library
R.S.M.A.S.
University of Miami
4600 Rickenbacker Causeway
Miami, FL 33149

Maury Oceanographic Library
Naval Oceanographic Office
Bay St. Louis
NSTL, MS 39522-5001

Marine Sciences Collection
Mayaguez Campus Library
University of Puerto Rico
Mayagues, Puerto Rico 00708

50272-101

REPORT DOCUMENTATION PAGE	1. REPORT NO. WHOI-89-11(CRC-89-3)	2.	3. Recipient's Accession No.

4. Title and Subtitle

The 17-Meter Flume at the Coastal Research Laboratory.
Part II: Flow Characteristics

5. Report Date
May 1989

6.

7. Author(s)
John H. Trowbridge, W. Rockwell Geyer, Cheryl Ann Butman and Robert J. Chapman

8. Performing Organization Rept. No.
WHOI-89-11

9. Performing Organization Name and Address

The Woods Hole Oceanographic Institution
Woods Hole, Massachusetts 02543

10. Project/Task/Work Unit No.

11. Contract(C) or Grant(G) No.
(C) 14-12-0001-30262
(G) NA86-AA-D-SG090
N00014-86-K-0579

12. Sponsoring Organization Name and Address
Minerals Management Service; Sea Grant; and the Office of Naval Research Young Investigator Program

13. Type of Report & Period Covered
Technical Report

14.

15. Supplementary Notes

This report should be cited as: Woods Hole Oceanog. Inst. Tech. Rept., WHOI-89-11. CRC-89-3.

16. Abstract (Limit: 200 words)

This report summarizes the characteristics of the idealized one-dimensional turbulent channel flow for which the 17-Meter Flume was designed, and describes a measurement program designed to determine whether the flume can in fact produce such a flow. The measured quantities include mean velocities, Reynolds stresses, turbulence intensities and velocity spectra. Measured profiles of mean velocity, Reynolds stress and turbulence intensity are consistent with previous theoretical and empirical results. Measured spectra, although consistent with expectations over a wide range of frequencies, indicate a few unexpected features, including a constant spectral density at high frequencies (possibly due to aliasing or high-frequency noise), motion at a few well-defined high frequencies of order 10 hz (possibly due to structural vibrations), oscillations with time scales of order 30 s (possibly due to low-mode standing surface waves) and irregular motions with time scales of several minutes (possibly due to fluctuations in pump performance). The unexpected features indicated by the spectra at high and low frequencies do not have a significant effect on mean velocities and low-order statistics, but they may be important in some applications.

17. Document Analysis a. Descriptors

1. turbulent channel flow
2. boundary layer
3. flow measurements

b. Identifiers/Open-Ended Terms

c. COSATI Field/Group

18. Availability Statement	19. Security Class (This Report)	21. No. of Pages
Approved for publication; distribution unlimited.	UNCLASSIFIED	37
	20. Security Class (This Page)	22. Price